How to cite: Angew. Chem. Int. Ed. 2023, e202307365
doi.org/10.1002/anie.202307365

Zn-Organic Batteries

In Situ Electrochemical Activation of Hydroxyl Polymer Cathode for High-Performance Aqueous Zinc–Organic Batteries

Qi-Qi Sun, Tao Sun, Jia-Yi Du, Zi-Long Xie, Dong-Yue Yang, Gang Huang, Hai-Ming Xie,* and Xin-Bo Zhang**

Abstract: The slow reaction kinetics and structural instability of organic electrode materials limit the further performance improvement of aqueous zinc-organic batteries. Herein, we have synthesized a Z-folded hydroxyl polymer polytetrafluorohydroquinone (PTFHQ) with inert hydroxyl groups that could be partially oxidized to the active carbonyl groups through the in situ activation process and then undertake the storage/release of Zn^{2+}. In the activated PTFHQ, the hydroxyl groups and S atoms enlarge the electronegativity region near the electrochemically active carbonyl groups, enhancing their electrochemical activity. Simultaneously, the residual hydroxyl groups could act as hydrophilic groups to enhance the electrolyte wettability while ensuring the stability of the polymer chain in the electrolyte. Also, the Z-folded structure of PTFHQ plays an important role in reversible binding with Zn^{2+} and fast ion diffusion. All these benefits make the activated PTFHQ exhibit a high specific capacity of 215 $mAh\,g^{-1}$ at 0.1 $A\,g^{-1}$, over 3400 stable cycles with a capacity retention of 92 %, and an outstanding rate capability of 196 $mAh\,g^{-1}$ at 20 $A\,g^{-1}$.

[*] Q.-Q. Sun,[+] J.-Y. Du,[+] Z.-L. Xie, D.-Y. Yang, Prof. G. Huang, Prof. X.-B. Zhang
State Key Laboratory of Rare Earth Resource Utilization, Changchun Institute of Applied Chemistry, Chinese Academy of Sciences
Changchun 130022 (China)
E-mail: ghuang@ciac.ac.cn
xbzhang@ciac.ac.cn

Q.-Q. Sun,[+] Prof. H.-M. Xie
National & Local United Engineering Laboratory for Power Battery, Department of Chemistry, Northeast Normal University
Changchun, Jilin 130024 (China)
E-mail: xiehm136@nenu.edu.cn

Prof. T. Sun[+]
Institute of Quantum and Sustainable Technology, School of Chemistry and Chemical Engineering, Jiangsu University
Zhenjiang 212013 (China)

J.-Y. Du,[+] Z.-L. Xie, D.-Y. Yang, Prof. G. Huang, Prof. X.-B. Zhang
School of Applied Chemistry and Engineering, University of Science and Technology of China
Hefei 230026 (China)

Introduction

The proposal of "carbon peak and neutrality" makes the development and large-scale application of renewable energy is in sore need of energy storage technology with higher safety and environmental sustainability.[1–4] Lithium-ion battery is the most mature type of energy storage system at present. However, the limited lithium resources and potential safety problems hinder its application in large-scale energy storage.[5–8] Among the existing energy storage systems, aqueous zinc-ion batteries (AZIBs) become a favorable choice owing to the inherent merits of Zn anodes, such as high capacity (820 $mAh\,g^{-1}$) and low redox potential (−0.762 V against standard hydrogen electrode), as well as the high safety, non-toxic, and low cost of aqueous electrolyte.[9–13] At present, the research on the cathode material of AZIBs is mainly based on manganese oxides,[14–15] vanadium oxides,[16–17] and Prussian blue analogs,[18] following an inorganic intercalation/conversion mechanism, which often leads to slow kinetics and poor cycling stability due to the structure collapse and irreversible active material dissolution during the discharge/charge process.[19] Hence, it is highly desirable to design a kind of host materials with flexible structures for adaptive Zn^{2+} storage/release and rapid Zn^{2+} migration.

Organic electrode materials (OEMs), as potential alternatives, are composed of naturally abundant elements (such as C, H, O, N, or S), possessing distinct advantageous characteristics, such as resource renewability, structural diversity, and design flexibility. More importantly, OEMs consisting of weak intermolecular interactions exhibit weak Coulomb repulsion to the diffused cations.[20–27] Meanwhile, the soft lattice and unique energy storage mechanism of OEMs could enable the reversible and facile Zn^{2+} storage/release. However, the inherent low conductivity and solubility of OEMs limit the realization of high-performance AZIBs. They usually need to be optimized by traditional methods, like extending the π-conjugated structure, recombining with a large amount of carbon matrix, and modifying the electrolyte.[28–33] Although these strategies could improve the battery performance to a certain extent, the most direct and effective strategy is to design advanced organic cathode materials with insoluble elastic structures to achieve stable storage/release and rapid diffusion of Zn^{2+}.

Polymer organic materials are ideal electrode materials due to their inherent insolubility and flexible polymer chains, which can provide stable skeletons and tunable internal space for highly reversible electrochemical reac-

tions. However, the hydrophobicity of the polymer backbone usually leads to slow ion transport, while the deprotonation of the polymer would result in severe deactivation in the weakly acidic electrolytes.[34] These problems restrict the full performance liberation of organic polymer electrodes in AZIBs. Besides, the existing research on polymer electrodes mainly focuses on the synthesis of new repeating units containing traditional active groups (such as carbonyl, amine, or thioether), whereas there are few studies on hydrophilic non-intrinsic electrochemically active functional groups. Realizing the conversion of inert functional groups to active ones to obtain electrochemical performance and good electrolyte wettability could play a synergistic role in accelerating the migration of ions.[35] At the same time, the design of polymer structure and the clarification of the energy storage mechanism are also very important for achieving excellent battery performance.

Based on these considerations, herein, we have designed a Z-folded hydroxyl polymer polytetrafluorohydroquinone (PTFHQ) as the cathode material for AZIBs. The PTFHQ was synthesized by a facile one-step reaction (Scheme 1) with a potential for large-scale production. The simple unbranched structure of PTFHQ could avoid the high entanglement of polymer chains, which is conducive to the full exposure of active sites. In theory, the hydroxyl group cannot achieve the storage/release of Zn^{2+} through the change of its covalent state; that is, the hydroxyl group itself has non-electrochemical activity. However, it is found that the hydroxyl in PTFHQ could be partially oxidized to the active carbonyl with the ability to combine with Zn^{2+} after the in situ activation process.[36–39] Meanwhile, the residual hydroxyl groups can be used as proton carriers to ensure the activity of PTFHQ in the weak acidic electrolyte. And as a kind of hydrophilic group, they could also increase the hydrophilicity of the material and then accelerate the transport of Zn^{2+}. More importantly, the presence of the multifunctional groups (C=O, –OH, and –S–) enhances the redox activity of the activated PTFHQ. As a result, it shows superior electrochemical performance when compared with the reported carbonyl polymers: a high reversible capacity of 215 mAh g^{-1} at 0.1 A g^{-1}, long-term cycling of 3400 cycles with a capacity retention of 92.0%, and an ultrafast rate capability of 196 mAh g^{-1} at 20 A g^{-1}. The research in this paper provides ideas for the design and application of polymer organic electrode materials for constructing high-performance AZIBs.

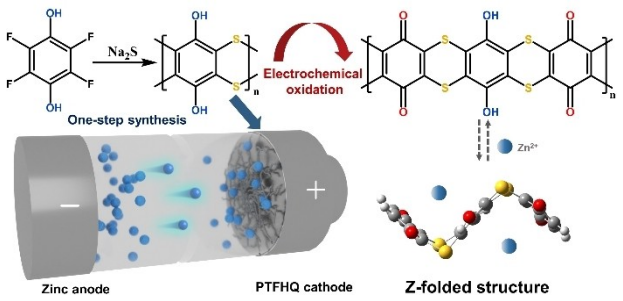

Scheme 1. The synthesis of PTFHQ and proposed redox mechanism for AZIBs.

Results and Discussion

The PTFHQ was prepared by a one-step polymerization reaction according to the method reported in previous literature.[40] As indicated in Figure S1a, the characteristic peak of the Fourier transform infrared (FTIR) spectrum at 3448 cm^{-1} can be attributed to the stretching vibrations of the –OH groups. The peaks at 1420, 1380, and 1068 cm^{-1} can be ascribed to the stretching vibrations of C–S, indicating the existence of thioether bond (C–S–C). For the absorption peak at 1527 cm^{-1}, it belongs to the C=C stretching vibrations. And the strong peak at 1176 cm^{-1} corresponds to the stretching vibration of C–O. All these confirm that the synthesized polymer only contains the stretching vibrations of PTFHQ without any impurity peaks. The X-ray diffraction (XRD) pattern reveals that the PTFHQ has certain crystallinity compared with the majority of polymers (Figure S1b). In addition, the successful synthesis of high-purity PTFHQ could be further verified by solid-state ^{1}H NMR and ^{13}C NMR (Figure S1c–d). The scanning electron microscopy (SEM) image shows the particle-type PTFHQ with a size in the range of 0.3 to 3 μm (Figure S2), and the EDS elemental mapping reveals the even distribution of C, O, and S elements in the skeleton of PTFHQ (Figure S3). For the initial raw material Tetrafluorohydroquinone (TFHQ), it easily dissolves in the electrolyte and loses its electrochemical performance with a rather limited capacity (Figure S4). While for PTFHQ, potentially stable electrochemical capability might be achieved by the polymerization of TFHQ through the linking of sulfur atoms. Figure 1a shows the CV curves of PTFHQ at different cycles in 2 M $Zn(CF_3SO_3)_2$. The 5th CV curve exhibits two oxidation peaks around 1.10 V and 1.35 V and one reduction peak at 0.92 V. In the following cycles (Figure S5), the gradual weakening of the high potential oxidation peak and the enhancement of a couple of reversible redox peaks can be observed simultaneously. The irreversible oxidation peak at the high potential corresponds to the oxidation process of the hydroxyl groups, while the remaining pair of reversible redox peaks can be ascribed to the storage/release of Zn^{2+} with the oxidized form of hydroxyl groups. Only a pair of redox peaks (0.96 V/1.10 V) remains after about 20 cycles, indicating the completion of the electrochemical oxidation process of hydroxyl groups. The charge/discharge curves are in agreement with the CV results and the PTFHQ||Zn cell delivers a specific capacity of 215 mAh g^{-1} after the completion of the in situ activation process (Figure 1b). To demonstrate the in situ electrochemical activation mechanism from an electrochemical point of view, we conducted charging-first and discharging-first tests on the fresh cells, respectively. As shown in Figure S6, the PTFHQ has almost no capacity if discharging first and can only exert reversible electrochemical performance after charging (or charging-first). In addition, the specific capacity increased with the deepening of the in situ activation. The electro-

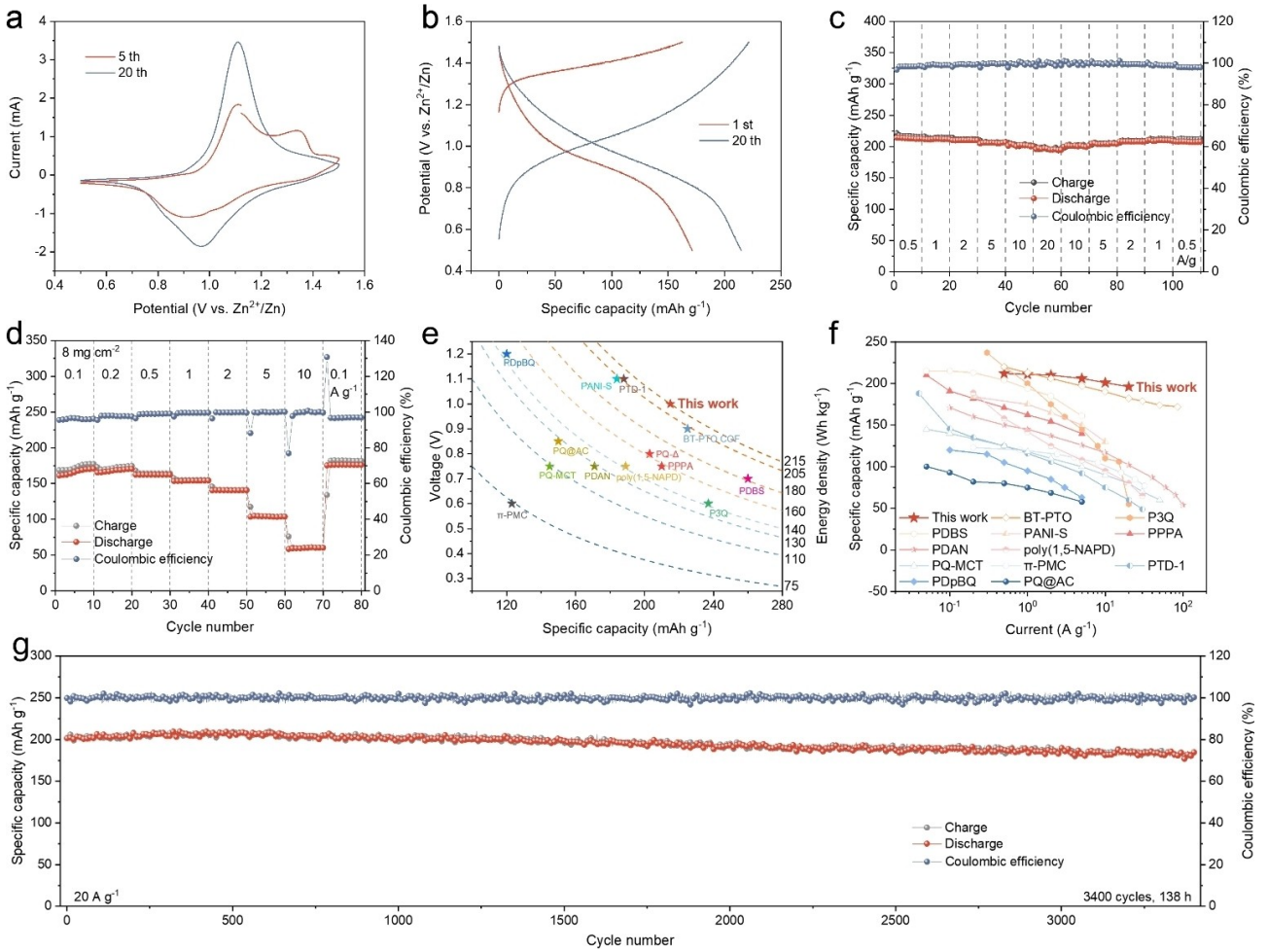

Figure 1. Electrochemical performance of PTFHQ||Zn cell in 2 M $Zn(CF_3SO_3)_2$. (a) CV curves at 0.5 mV s^{-1}. (b) Discharge/charge curves at a current density of 0.1 A g^{-1}. Rate performance with mass loadings of (c) 1.3 mg cm^{-2} and (d) 8 mg cm^{-2}. The comparison of (e) electrochemical performance and (f) rate capability of aqueous ZIBs with different OEMs. (g) Cycling performance at 20 A g^{-1}.

chemical impedance spectroscopy (EIS) measurement was also performed to study the in situ electrochemical activation process induced impedance change for PTFHQ and PTFHQ-A (Figure S7). It is clear that the charge transfer impedance (R_{ct}) decreases significantly after activation, which is probably due to the activation rendered electrical conductivity improvement for PTFHQ-A (consistent with the following theoretical calculation results). The subsequent electrochemical tests and correlation characterizations were carried out after the activation process (remarked as PTFHQ-A) unless otherwise noted.

Benefiting from the existence of sulfur atoms and –OH,[41] the charge/discharge profiles of PTFHQ-A achieve a high average voltage of 1.0 V (Figure 1b). In Figure 1c, an outstanding rate performance of the PTFHQ-A is also realized. With the increase of current densities to 1, 2, 5, 10, and 20 A g^{-1}, capacities of 211, 210, 206, 201, and 196 mAh g^{-1} are delivered, respectively. This superior rate capability is related to the rapid reaction kinetic of PTFHQ-A and will be discussed later. Even at a high mass loading of 8 mg_{PTFHQ} cm^{-2}, the PTFHQ-A could still render capacities of 170, 170, 162, 154, 140, and 103 mAh g^{-1} at 0.1, 0.2, 0.5, 1, 2, and 5 A g^{-1}, respectively, and finally recovers to 176 mAh g^{-1} at 0.1 A g^{-1} (Figure 1d). Importantly, the severe electrochemical polarization and voltage drop are not observed even under fast discharge/charge conditions (Figure S8). Moreover, we also conducted the rate performance tests at a higher current density and also at a large mass loading. As shown in Figure S9a, the PTFHQ could complete a rapid discharge/charge process in 22 s and delivers a specific capacity of 145 mAh g^{-1} at 50 A g^{-1}. Also, acceptable rate performance could still obtain at a high mass loading of 15 mg_{PTFHQ} cm^{-2} (Figure S9b). As depicted in Figure 1e and S10, the energy density of PTFHQ-A exceeds most of the reported organic cathode materials (based on the mass of the cathode). And the excellent rate performance achieved here is difficult to obtain in other organic cathode materials (Figure 1f).[29,31,33,36,37,42–48] Besides, the long-term cycling test of PTFHQ-A at 20 A g^{-1} was conducted (Figure 1g). The battery delivers a capacity of 196 mAh g^{-1} with a capacity retention of 92 % over 3400 cycles (138 h). The longer lifetime of PTFHQ-A has also been confirmed under other

current densities (Figure S11). These results confirm that the rational design of polymer electrodes is an effective method to obtain excellent rate capability and improve electrochemical stability.

In order to gain a deeper insight into the reasons for the exceptional rate performance, the reaction kinetic analysis of PTFHQ-A was carried out. From Figure 2a we can see that a pair of redox peaks in the CV curves could be well maintained even with the increase of scan rate from 0.1 to 2.0 mV s^{-1}. According to the equation as follows:

$$i = av^b \tag{1}$$

the calculated b-values of the anodic and cathodic peaks are 0.855 and 0.809 (close to 1), which implies that the redox reaction of PTFHQ-A is mainly controlled by the capacitive process (Figure 2b). Furthermore, the percentage of capacity contributed by the capacitive process at a fixed scan rate is calculated by the following equation:

$$i = k_1 v + k_2 v^{1/2} \tag{2}$$

where $k_1 v$ represents the capacitive-controlled process and $k_2 v^{1/2}$ is diffusion-controlled reaction. The high capacitive contribution ratios at different scan rates further prove the fast reaction kinetics of PTFHQ-A (Figure 2c–d). Although the energy storage in PTFHQ-A is mainly dominated by the capacitance process, the "pseudo-capacitance" process in OEMs is based on the redox reaction accompanied by ion storage/release, and the diffusion of ions in the electrode is the rate-limiting step. Therefore, the diffusion coefficient (D) of Zn^{2+} was estimated by the galvanostatic intermittent titration technique (GITT) to study its diffusion dynamics in PTFHQ-A (Figure 2e). The calculation method of diffusion coefficients is based on the following equation:

$$D = \frac{4}{\pi\tau}\left(\frac{m_B V_M}{M_B S}\right)^2 \left(\frac{\Delta E_S}{\Delta E_\tau}\right)^2 \tag{3}$$

Where m_B, V_M, and M_B represent the mass, molar volume, and molecular weight; τ is the duration time of a pulse; S is the contact area of electrode-electrolyte; ΔE_τ and ΔE_s represent the changes of battery voltage and quasi-balanced voltage, respectively. The high charge capacity in the GITT curve is due to the sufficient oxidation of the hydroxyl groups under the repeated resting steps with a low current density of 0.02 A g^{-1}. Figure 2f shows the diffusion coefficient $D_{Zn^{2+}}$ ranges from 10^{-10} to 10^{-11} $cm^2 s^{-1}$. During the charge process, the D value drops from the maximum 4.5×10^{-10} $cm^2 s^{-1}$ and stabilizes around 10^{-11} $cm^2 s^{-1}$. For the discharge process, the D value decreases from 4.5×10^{-10} to 10^{-10} $cm^2 s^{-1}$. It should be mentioned that the $D_{Zn^{2+}}$ for most of the reported OEMs is in the 10^{-12} level, so this rapid diffusion of Zn^{2+} is undoubtedly the reason for the remarkable rate performance of PTFHQ-A (Table S1).

Based on the above studies on the electrochemical behavior, we further conducted an in-depth analysis of the energy storage mechanism of PTFHQ. As illustrated in Scheme 1, the PTFHQ is activated by the gradual oxidation of hydroxyl groups to carbonyl groups during the initial

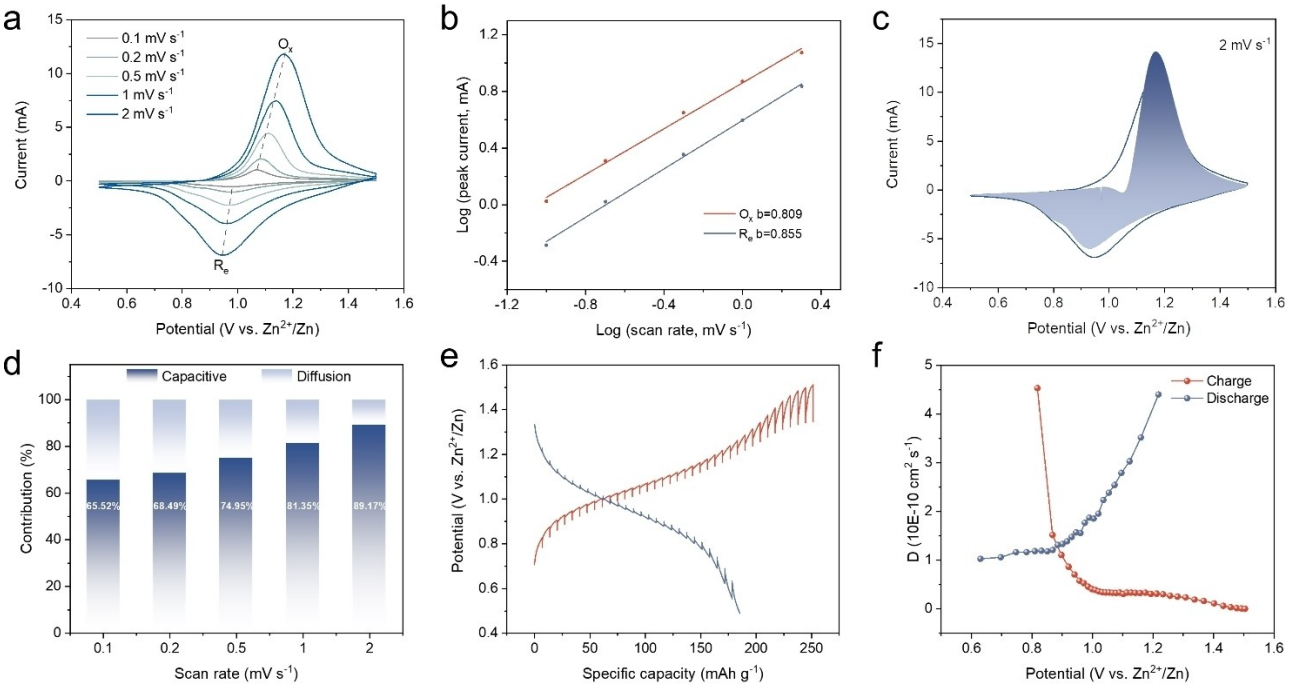

Figure 2. Reaction kinetic analysis of PTFHQ-A in 2 M $Zn(CF_3SO_3)_2$. (a) CV curves at different scan rates. (b) Power law dependence of the measured current on scan rate at corresponding peak potentials. (c) Capacitive contribution at 2 mV s^{-1}. (d) Relative contributions of the capacitive and diffusion-controlled charge storage at different scan rates. (e) GITT curve of PTFHQ-A. (f) Diffusion coefficient (D) estimated from GITT method.

charge process. The activated PTFHQ will store and release Zn^{2+} in enolization form during the subsequent discharge/charge processes. The electrochemical test has confirmed that the fresh PTFHQ proceeds an electrochemical oxidation process at the first charge process and completes the in situ activation within 20 cycles at 0.1 $A g^{-1}$ (Figure 1b). The composition change of PTFHQ during the in situ electrochemical activation process was investigated by X-ray photoelectron spectroscopy (XPS) in Figure 3a, 3b, and S12. In the O 1s region, the intensity of the C=O peak gradually enhances with the cycling process, and its relative content stabilizes at 70 % after 20 cycles, confirming the conversion of the hydroxyl to carbonyl with 30 % residual hydroxyl. We further analyzed the structural changes of PTFHQ during the activation process by FTIR. The C=O peak appears with gradually increased intensity, while the significant decrease in the relative intensity of –OH peak is also observed in the ex-FTIR spectra during the in situ activation process (Figure S13). The presence of the residual hydroxyl groups could play important roles in improving the electrochemical performance. First of all, the hydroxyl group can increase the activity of carbonyl to accelerate the enolization process.[41] Secondly, since the deprotonation of polymers in the low pH electrolyte tends to lead to polymer deactivation,[34] the hydroxyl group as a proton carrier can ensure that the polymer does not lose activity in the weak acid electrolyte and improve the stability of PTFHQ. Finally, the hydroxyl group as a hydrophilic group can increase the compatibility between the polymer and the aqueous electrolyte and then accelerates the ion diffusion rate. All these reveal the indispensable functions of the residual hydroxyl groups in enabling the PTFHQ-A to liberate the full performance.

To demonstrate the superiority of the in situ electrochemical activation of the hydroxyl in PTFHQ, poly(2,3-dithiino-1,4-benzoquinone) (PDB), a "fully carbonylated PTFHQ", was synthesized by the same chemical synthesis method as a control sample (Scheme S1), and basic electrochemical tests were conducted. As shown in Figure S14a, the PDB has a pair of redox peaks at 1.0 V/1.1 V, which is consistent with the pair of reversible redox peaks of PTFHQ. This can also prove that the oxidation peak at the high potential of PTFHQ is derived from the electrochemical oxidation of hydroxyl groups. We know that the theoretical specific capacity of a polymer electrode material could be calculated according to Eq. (4):

$$C = \frac{nF}{3.6M} \tag{4}$$

Where n is the number of transferred electrons in a repeating unit, F is the Faraday constant, and M is the molecular mass of the repeating unit of polymers. The PDB has a higher theoretical specific capacity of 319 $mAh g^{-1}$ than PTFHQ-A (223 $mAh g^{-1}$, according to the actual content of carbonyl groups). But in fact, the PDB could only display a specific capacity of 127 $mAh g^{-1}$ with an active group utilization rate of 40 % (Figure S14b), much lower than that of PTFHQ-A (96 %). At the same time, the PDB also exhibits poor rate capability and cycle performance (inactivation just after 108 cycles) (Figure S14c–d). The poor electrolyte wettability of PDB may be one of the reasons for

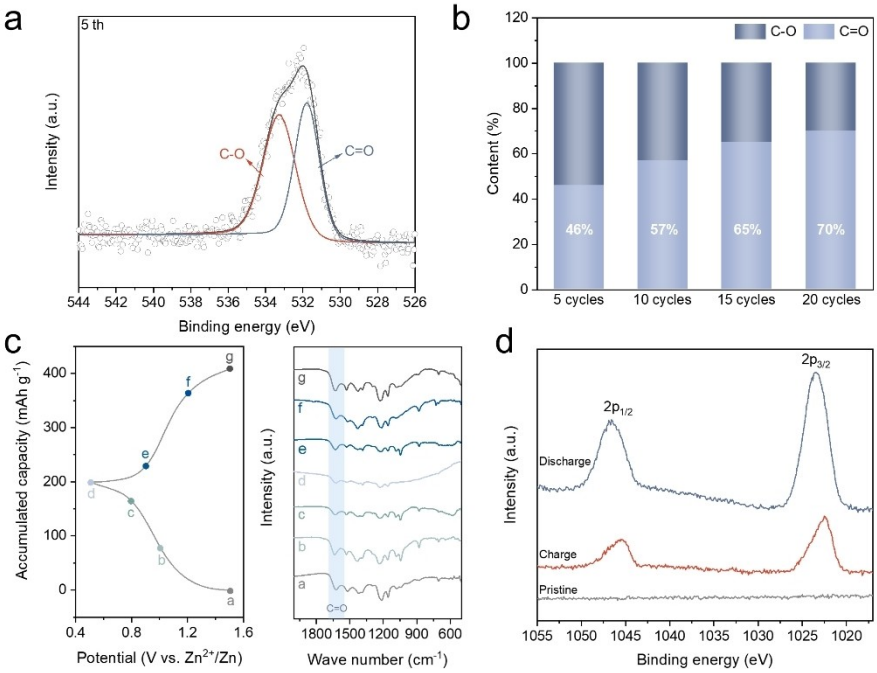

Figure 3. Study on the energy storage mechanism of PTFHQ. (a) XPS spectrum of O 1s region for PTFHQ after 5 cycles. (b) Evolution of the carbonyl content from the ex situ XPS spectra recorded at the initial cycling. (c) Ex situ FTIR spectra recorded at various electrochemical states. (d) XPS spectra of Zn 2p at pristine, fully discharged, and charged states.

its inferior electrochemical performance (Figure S15). These results demonstrate that the existence of residual hydroxyl groups greatly enhances the utilization of active groups, ionic diffusion, and the stability of the polymers in the weakly acidic solutions.

FTIR was then conducted to prove the reversible enolization of C=O in PTFHQ-A during the discharge/charge process. The FTIR spectra were collected at different charge/discharge states within one cycle to demonstrate the evolution of carbonyl groups (Figure 3c, S16). During the discharge process, the C=O peak at 1620 cm^{-1} gradually weakens and reaches the weakest intensity in the fully discharged state. The intensity of this peak gradually recoveries to the initial value during the recharge process, demonstrating the reversible storage of Zn^{2+} by the C=O groups. This again confirms our proposed mechanism of in situ activating the hydroxyl groups in PTFHQ, and a reversible redox reaction can be realized through the enolization of the carbonyl groups. The XPS result also further verifies the storage/release of Zn^{2+} in the PTFHQ-A (Figure 3d). In the Zn 2p region, the strong peaks at the fully discharged state indicate the storage of Zn^{2+}, and the significant decrease in the intensity of these peaks at the charged state is due to the Zn^{2+} extraction from PTFHQ-A. This is consistent with the FTIR analysis and confirms the reversible electrochemical reaction of the C=O groups after in situ activation. In addition, the discharge/charge tests of PTFHQ-A were also conducted in 0.3 M $Zn(CF_3SO_3)_2$/acetonitrile ($Zn(CF_3SO_3)_2$/AN) and 1 M H_2SO_4 electrolytes, respectively. In Figure S17, the PTFHQ delivers a specific capacity of 198 mAh g^{-1} in 0.3 M $Zn(CF_3SO_3)_2$/AN electrolyte, and it only has a specific capacity of 48 mAh g^{-1} in 1 M H_2SO_4 electrolyte, indicating that the Zn^{2+} storage dominates the overall electrochemical reaction in PTFHQ, while H^+ just partially involves the energy storage process. Furthermore, considering the H^+ concentration in 2 M $Zn(CF_3SO_3)_2$ is rather limited (pH ≈ 4), the capacity contribution from H^+ could be reasonably ignored.

The electrochemical reaction mechanism of organic electrode materials is the coordination interaction between the cations and active sites. The uptake of Zn^{2+} can be considered as an electrophilic reaction, which is more inclined to occur at positions with higher electronegativity. In this consideration, the active centers of PTFHQ-A were predicted based on theoretical calculations. In order to reasonably speculate the reaction mechanism of PTFHQ-A, its polymer unit model was established according to the contents of hydroxyl groups after the in situ activation process. In Figure 4a, the molecular electrostatic potential (ESP) mapping of PTFHQ-A shows that a large part of the electron density is distributed between S atoms, carbonyl and hydroxyl groups. This indicates that the Zn^{2+} has a large electronegative binding region, which is conducive to fully utilizing the active sites. The calculation of energy levels of PTFHQ and PTFHQ-A was also conducted. As shown in Figure S18a, the PTFHQ-A has a lower LUMO energy of −4.039 eV than that of PTFHQ (−1.411 eV). This reveals that the activated PTFHQ-A has a strong electron affinity and is easier to obtain electrons for redox reactions. More importantly, the significantly narrower band gap (ΔE) of PTFHQ-A than PTFHQ (2.237 vs. 4.336 eV) indicates that it has a small energy barrier, facilitating efficient electron conduction. In addition, to fully explain the role of the activation process, we have calculated the free energy changes (ΔG) of PTFHQ and PTFHQ-A after accepting two electrons, respectively. From Figure S18b we can see that the structure of PTFHQ-A remains basically unchanged after receiving two electrons with a ΔG of −8.289 eV. While

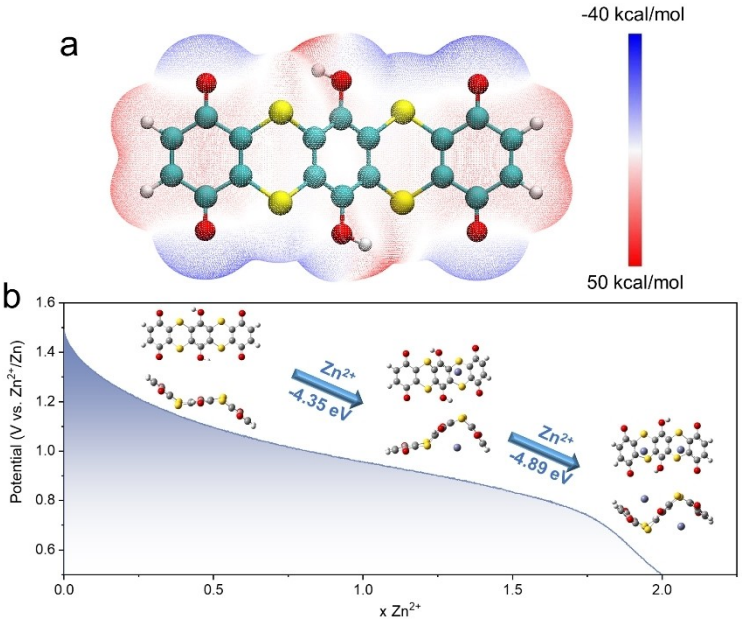

Figure 4. Theoretical calculation of PTFHQ-A. (a) The ESP mapped molecular van der Waals surface of PTFHQ-A. (b) The optimized geometries and relative Gibbs energies (ΔG) of PTFHQ-A, PTFHQ-A(Zn^{2+}), and PTFHQ-A(Zn^{2+})$_2$.

for PTFHQ, its structure collapses with a positive ΔG value after receiving two electrons. These results fully prove that the PTFHQ can only obtain electrons after activation, which is highly consistent with our electrochemical test results. To further investigate the energy storage process of PTFHQ-A, the changes in the chain configuration during Zn^{2+} uptake were investigated. The possible binding forms of Zn^{2+} were considered and optimized (Figure S19–S20), and the most reasonable binding process was screened out according to the Gibbs energy change (Figure 4b). In Figure 4b, it can be seen that the uptake of Zn^{2+} basically maintains the original Z-folded structure of PTFHQ-A. In terms of spatial structure, the Zn^{2+} after coordination with the carbonyl groups is located in the Z-folded structure of two adjacent benzene rings that are connected by S atoms, and this unique spatial structure is conducive to the rapid diffusion of Zn^{2+}. This result is also consistent with the above ESP analysis. Such Zn^{2+} storage status is more favorable for the rapid diffusion of ions in the flexible polymer chains. The active region composed of various functional groups and the Z-folded structure together endow the PTFHQ with excellent electrochemical performance.

Conclusion

In conclusion, we have designed a hydroxyl polymer PTFHQ as electrode material for constructing high-performance aqueous Zn-organic batteries. In PTFHQ, the hydroxyl groups could partially convert to carbonyl groups by an in situ electrochemical activation process and then participate in the storage/release of Zn^{2+} by enolization. Meanwhile, the remaining hydroxyl groups can increase the stability of the polymer in the weak acid aqueous electrolyte and enhance the electrolyte wettability of the electrode with accelerated ion diffusion. Most importantly, the multifunctional group composition of the PTFHQ-A constitutes a larger electronegativity region, which makes the Zn^{2+} fully coordinate with the exposed active sites. Benefiting from these advantages and together with the stability and flexibility of the Z-folded structure, the PTFHQ-A has demonstrated a specific capacity of 215 $mAh\,g^{-1}$ at 0.1 $A\,g^{-1}$, an outstanding rate capability with a capacity retention of 91 % at 20 $A\,g^{-1}$, and a remarkable cycle stability (capacity retention of 92 % over 3400 cycles). Our results extend the understanding of the reaction mechanism in Zn-organic batteries and provide new design directions for polymers to enable efficient Zn^{2+} storage.

Acknowledgements

This work was financially supported by the National Key R&D program of China (Grant 2022YFB2402200), National Natural Science Foundation of China (Grant 52271140, 52171194), Changchun Science and Technology Development Plan Funding Project (Grant 21ZY06), and Youth Innovation Promotion Association CAS (Grant 2020230).

Conflict of Interest

The authors declare no conflict of interest.

Data Availability Statement

The data that support the findings of this study are available from the corresponding author upon reasonable request.

Keywords: High Rate · Hydroxyl Polymer · Organic Electrodes · Zn-Ion Batteries · In Situ Electrochemical Activation

[1] S. S. Sharma, A. Manthiram, *Energy Environ. Sci.* **2020**, *13*, 4087.
[2] S. Chu, A. Majumdar, *Nature* **2012**, *488*, 294.
[3] M. H. Lee, J. Lee, S. K. Jung, D. Kang, M. S. Park, G. D. Cha, K. W. Cho, J. H. Song, S. Moon, Y. S. Yun, S. J. Kim, Y. W. Lim, D. H. Kim, K. Kang, *Adv. Mater.* **2021**, *33*, 2004902.
[4] D. Larcher, J.-M. Tarascon, *Nat. Chem.* **2015**, *7*, 19.
[5] Y. Lu, J. Chen, *Nat. Chem. Rev.* **2020**, *4*, 127.
[6] M. Winter, B. Barnett, K. Xu, *Chem. Rev.* **2018**, *118*, 11433.
[7] M. Li, J. Lu, Z. Chen, K. Amine, *Adv. Mater.* **2018**, *30*, 1800561.
[8] J. B. Goodenough, K.-S. Park, *J. Am. Chem. Soc.* **2013**, *135*, 1167.
[9] J. Huang, X. Dong, Z. Guo, Y. Wang, *Angew. Chem. Int. Ed.* **2020**, *59*, 18322.
[10] X. Zeng, J. Hao, Z. Wang, J. Mao, Z. Guo, *Energy Storage Mater.* **2019**, *20*, 410.
[11] L. E. Blanc, D. Kundu, L. F. Nazar, *Joule* **2020**, *4*, 771.
[12] L. Ma, M. A. Schroeder, O. Borodin, T. P. Pollard, M. S. Ding, C. Wang, K. Xu, *Nat. Energy* **2020**, *5*, 743.
[13] Y. Wang, J. Yin, J. Zhu, *Chin. J. Chem.* **2022**, *40*, 973.
[14] D. Chao, W. Zhou, C. Ye, Q. Zhang, Y. Chen, L. Gu, K. Davey, S.-Z. Qiao, *Angew. Chem. Int. Ed.* **2019**, *58*, 7823.
[15] H. Pan, Y. Shao, P. Yan, Y. Cheng, K. S. Han, Z. Nie, C. Wang, J. Yang, X. Li, P. Bhattacharya, K. T. Mueller, J. Liu, *Nat. Energy* **2016**, *1*, 16039.
[16] Z. Li, S. Ganapathy, Y. Xu, Z. Zhou, M. Sarilar, M. Wagemaker, *Adv. Energy Mater.* **2019**, *9*, 1900237.
[17] L. L. Wang, K. W. Huang, J. T. Chen, J. R. Zheng, *Sci. Adv.* **2019**, *5*, eaax4279.
[18] G. Du, H. Pang, *Energy Storage Mater.* **2021**, *36*, 387.
[19] H. Liang, Z. Cao, F. Ming, W. Zhang, D. H. Anjum, Y. Cui, L. Cavallo, H. N. Alshareef, *Nano Lett.* **2019**, *19*, 3199.
[20] K. Qin, J. Huang, K. Holguin, C. Luo, *Energy Environ. Sci.* **2020**, *13*, 3950.
[21] Y. Liang, Y. Yao, *Joule* **2018**, *2*, 1690.
[22] S. Lee, J. Hong, K. Kang, *Adv. Energy Mater.* **2020**, *10*, 2001445.
[23] S. Lee, G. Kwon, K. Ku, K. Yoon, S.-K. Jung, H.-D. Lim, K. Kang, *Adv. Mater.* **2018**, *30*, 1704682.
[24] P. Poizot, J. Gaubicher, S. Renault, L. Dubois, Y. Liang, Y. Yao, *Chem. Rev.* **2020**, *120*, 6490.
[25] W. Du, X. Du, M. Ma, S. Huang, X. Sun, L. Xiong, *Adv. Funct. Mater.* **2022**, *32*, 2110871.
[26] W. Yang, X. Du, J. Zhao, Z. Chen, J. Li, J. Xie, Y. Zhang, Z. Cui, Q. Kong, Z. Zhao, C. Wang, Q. Zhang, G. Cui, *Joule* **2020**, *4*, 1557.
[27] X. Sun, X. Yan, K. Song, T. Zhang, Z. Yang, X. Su, W. Chen, L. Chen, *Chin. J. Chem.* **2023**, *41*, 1691.
[28] Y. Zhao, Y. Huang, F. Wu, R. Chen, L. Li, *Adv. Mater.* **2021**, *33*, 2106469.

[29] N. Wang, Z. Guo, Z. Ni, J. Xu, X. Qiu, J. Ma, P. Wei, Y. Wang, *Angew. Chem. Int. Ed.* **2021**, *60*, 20826.
[30] Z. Song, L. Miao, H. Duan, L. Ruhlmann, Y. Lv, D. Zhu, L. Li, L. Gan, M. Liu, *Angew. Chem. Int. Ed.* **2022**, *61*, e202208821.
[31] X. Wang, J. Tang, W. Tang, *Adv. Funct. Mater.* **2022**, *32*, 2200517.
[32] Y. Chen, J. Li, Q. Zhu, K. Fan, Y. Cao, G. Zhang, C. Zhang, Y. Gao, J. Zou, T. Zhai, C. Wang, *Angew. Chem. Int. Ed.* **2022**, *61*, e202116289.
[33] S. Zheng, D. Shi, D. Yan, Q. Wang, T. Sun, T. Ma, L. Li, D. He, Z. Tao, J. Chen, *Angew. Chem. Int. Ed.* **2022**, *61*, e202117511.
[34] N. M. Chola, R. K. Nagarale, *Batteries & Supercaps* **2022**, *5*, e202200221.
[35] Z. Chen, H. Su, P. Sun, P. Bai, J. Yang, M. Li, Y. Deng, Y. Liu, Y. Geng, Y. Xu, *Proc. Natl. Acad. Sci. USA* **2022**, *119*, e2116775119.
[36] T. Sun, Z. J. Li, Y. F. Zhi, Y. J. Huang, H. J. Fan, Q. Zhang, *Adv. Funct. Mater.* **2021**, *31*, 2010049.
[37] X. Wang, J. Xiao, W. Tang, *Adv. Funct. Mater.* **2021**, *32*, 2108225.
[38] Y. Shi, J. Yang, J. Yang, Z. Wang, Z. Chen, Y. Xu, *Adv. Funct. Mater.* **2022**, *32*, 2111307.
[39] N. Patil, C. Cruz, D. Ciurduc, A. Mavrandonakis, J. Palma, R. Marcilla, *Adv. Energy Mater.* **2021**, *11*, 2100939.
[40] J. Xie, Z. Wang, Z. J. Xu, Q. Zhang, *Adv. Energy Mater.* **2018**, *8*, 1703509.
[41] H. Peng, Q. Yu, S. Wang, J. Kim, A. E. Rowan, A. K. Nanjundan, Y. Yamauchi, J. Yu, *Adv. Sci.* **2019**, *6*, 1900431.
[42] L. Yan, Q. Zhu, Y. Qi, J. Xu, Y. Peng, J. Shu, J. Ma, Y. Wang, *Angew. Chem. Int. Ed.* **2022**, *61*, e202211107.
[43] H. Zhang, Y. Fang, F. Yang, X. Liu, X. Lu, *Energy Environ. Sci.* **2020**, *13*, 2515.
[44] N. Wang, X. Dong, B. Wang, Z. Guo, Z. Wang, R. Wang, X. Qiu, Y. Wang, *Angew. Chem. Int. Ed.* **2020**, *59*, 14577.
[45] B. Yang, Y. Ma, D. Bin, H. Lu, Y. Xia, *ACS Appl. Mater. Interfaces* **2021**, *13*, 58818.
[46] F. Ye, Q. Liu, H. Dong, K. Guan, Z. Chen, N. Ju, L. Hu, *Angew. Chem. Int. Ed.* **2022**, *61*, e202214244.
[47] H.-Y. Shi, Y.-J. Ye, K. Liu, Y. Song, X. Sun, *Angew. Chem. Int. Ed.* **2018**, *57*, 16359.
[48] L. Yan, Y. Zhang, Z. Ni, Y. Zhang, J. Xu, T. Kong, J. Huang, W. Li, J. Ma, Y. Wang, *J. Am. Chem. Soc.* **2021**, *143*, 15369.

Manuscript received: May 25, 2023
Accepted manuscript online: July 9, 2023
Version of record online: ■■, ■■

Research Articles

Zn-Organic Batteries

Q.-Q. Sun, T. Sun, J.-Y. Du, Z.-L. Xie, D.-Y. Yang, G. Huang,* H.-M. Xie,* X.-B. Zhang* **e202307365**

In Situ Electrochemical Activation of Hydroxyl Polymer Cathode for High-Performance Aqueous Zinc–Organic Batteries

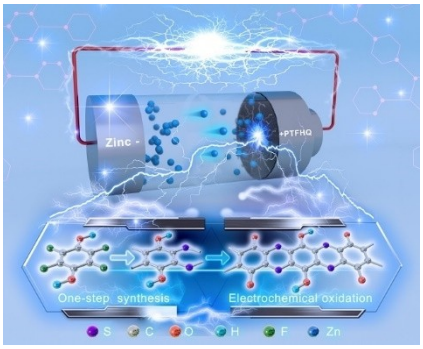

A hydroxyl polymer PTFHQ has been designed to obtain electrochemical activity through an in situ electrochemical activation process. The synergistic effects of the different functional groups (C=O, –OH, and –S–) and the unique Z-folded structure of the activated PTFHQ effectively improve its electrochemical activity and contribute to the rapid reaction kinetics, realizing the construction of high-performance zinc-organic batteries.